CONF-851007--11

START PAGE 2 AND SUBSEQUENT

TWO-PHASE GAS BUBBLE-LIQUID BOUNDARY LAYER FLOW ALONG VERTICAL AND INCLINED SURFACES

by

F. B. Cheung
Department of Mechanical Engineering
The Pennsylvania State University
University Park, PA 16802

M. Epstein
Fauske & Associates, Inc.
16W070 West 83rd Street
Burr Ridge, IL 60521

CONF-851007--11

DE85 018462

ABSTRACT

The behavior of a two-phase gas bubble-liquid boundary layer along vertical and inclined porous surfaces with uniform gas injection is investigated experimentally and analytically. Using argon gas and water as the working fluids, a photographical study of the two-phase boundary layer flow has been performed for various angles of inclination ranging from 45° to 135° and gas injection rates ranging from 0.01 to 0.1 m/s. An integral method has been employed to solve the system of equations governing the two-phase motion. The effects of the gas injection rate and the angle of inclination on the growth of the boundary layer have been determined. The predicted boundary layer thickness is found to be in good agreement with the experimental results. The calculated axial liquid velocity and the void fraction in the two-phase region are also presented along with the observed flow behavior.

1. INTRODUCTION

The interaction of molten core debris with concrete has been a key aspect of hypothetical core meltdown accidents in fast reactors. Previous studies [1,2] indicate that vigorous gas evolution occurs upon contact between the molten debris and concrete. The continuous release of gases at the concrete-melt interface results in a two-phase gas bubble-liquid boundary layer which in turn induces violent stirring of the liquid pool and thus strongly affects the heat transfer rate at the melting interface (see Figure 1). To understand the mechanism of pool growth into concrete, which constitutes the final line of defense against violation of the containment, the effect of gas release and the behavior of the two-phase boundary layer need to be studied.

A similar situation arises when a solid wall is in contact with liquid on one side and subjected to strong fluxes of energy through its thickness. In this case, a two-phase vapor-liquid boundary layer may develop due to the formation of vapor bubbles as active nuclei on the wall. These bubbles break away from the heated surface and rise along the wall, their drag on the liquid causing the liquid to move upward with the vapor as a free-convection boundary layer. Owing to the large density difference between the vapor and liquid phases, the bubble-induced liquid flow along the wall is usually much above that encountered during single-phase natural convection. The upward liquid velocity can become quite large compared with the terminal velocity of a single bubble.

While there is an extensive literature on the two-phase boundary layer for film boiling on vertical surfaces [3-6], relatively little previous work has been performed on free-convection boundary layers driven by gas bubbling or nucleate boiling. This is somewhat surprising considering the fact that nucleate boiling or gas bubbling from vertical or inclined walls occurs in a variety of industrial operations. Cumo et al. [7] have investigated two-phase boundary layers along heated walls, but their works deals exclusively with forced-convection flow of subcooled liquids. Most studies of two-phase free-convection flow have been restricted to buoyant plumes driven by rising gas bubbles through an isothermal or moderately stratified liquid environment [8-12]. It is the purpose of this study to investigate the behavior of a two-phase gas bubble-liquid free-convection boundary layer along vertical and inclined walls.

2. EXPERIMENTAL METHOD

The experimental apparatus consisted of a gas-injection unit constructed from a thick Plexiglas plate 38.1 cm high, 22.86 cm wide, and 5.08 cm thick, immersed in a relatively large volume of water contained in a 91-L aquarium (see Figure 2). Inside the Plexiglas unit, nine channels were machined, each 1.27 cm apart and 15.24 x 1.27 x 2.54 cm in size. A porous, sintered bronze plate, 0.3 cm thick, was bonded with aluminum-impregnated epoxy to a 0.64-cm-thick copper frame. The porous plate, having a cross-sectional area of 22.86 by 15.24 cm, was mounted in the Plexiglas unit above the nine channels, with a rubber gasket in between. The surfaces of the porous plate and the Plexiglas were in a common plane. Gas was supplied from a compressed-gas tank through a series of nine individual flowmeters to each channel in the Plexiglas. In this way, gas flow through each channel could be controlled independently. Fine metal screens were placed inside each channel to provide for uniform flow through the porous plate. The entire gas-injection unit was mounted on a rotating system sitting at the bottom of the aquarium. A vertical surface was obtained when

the system was rotated at $\theta = 90°$. For $\theta < 90°$, the plate was facing downward whereas for $\theta > 90°$, the plate was facing upward.

To prepare for a run, the gas-injection unit was rotated at the desired angle of inclination, θ. The aquarium was then filled with water at the room temperature, during which the gas supply was turned on and maintained at a low setting just to prevent water from getting into the flow channels. When the entire gas-injection unit was immersed in water, the gas valve was dialed to the prescribed setting and the nine individual flowmeters were adjusted so as to obtain a uniform flow through the porous plate. The water was slightly dyed green and the system was lightened to enhanced visual observations. After a short waiting period required to establish a steady-state flow condition, a series of pictures were taken. These were then enlarged to study the characteristics of the two-phase gas bubble-liquid boundary layer photographically.

3. OBSERVATIONS OF THE TWO-PHASE FREE-CONVECTION BOUNDARY LAYER

Experiments using argon gas and water as the working fluids were conducted with different values of gas injection rate ranging from 0.01 to 0.10 m/s and various angles of inclination ranging from 45 to 135°. In all these experiments, a free-convection boundary-layer-type bubbly-flow regime was observed in a region adjacent to the plate. The average bubble size ranged from 0.5 to 4 mm. Although bubbles did coalesce in the downstream locations, there was no formation of coherent gas film at the boundary over the range of gas injection rates explored in the experiment. It should be noted that there were strong recirculating currents away from the plate, apparently induced by the bubbly flow in the free-convection boundary layer. The level of pool mixing appeared to increase with the gas injection rate.

At a given gas injection rate, the behavior of the two-phase boundary layer depended strongly upon the angle of inclination of the plate, as illustrated in Figures 2 to 4. When the plate was facing upward with $\theta = 110°$ (Figure 2), the gas bubbles injected at the upstream locations were free to flow upward and they seldom coalesced with the gas bubbles released downstream. The bubbles rose uniformly and steadily along the plate, apparently in the ideal bubbly flow regime [13]. However, owing to liquid entrainment into the boundary layer from the liquid pool, the bubbles were pushed toward the inclined surface. Thus the outer edge of the gas bubble-liquid boundary layer was not vertical, but rather it was oriented in the same direction as the plate. As a result there was a slight increase in the average bubble size along the boundary layer. When the plate was vertical with $\theta = 90°$ (Figure 3), the situation is quite different. The gas bubbles injected at the upstream locations tended to coalesce with the bubbles released downstream, forming much larger bubbles. There was significant entrainment of bubbles in each other's wakes. The two-phase motion appeared to accelerate in the downstream direction. As a result, the flow pattern appeared to be agitated and unsteady. This condition became more severe when the plate was facing downward with $\theta = 70°$ (Figure 4). In this case, the average bubble size increased rapidly downstream due to bubble agglomeration. The two-phase motion was highly unsteady and was accelerating downstream. Apparently, the flow was in the churn-turbulent regime [13].

The observed boundary layer thickness along the plate is shown in Figure 5 for various angles of inclination. The shape of the boundary layer was determined from the enlarged photographs, ignoring the few individual bubbles that escaped outside the boundary layer. The gas injection rate was fixed at $j_g = 0.10$ m/s in all cases. When the plate was facing upward, the growth of the boundary layer appeared to accelerate in the downstream locations whereas it decelerated when the plate was facing downward. Thus the local boundary layer thickness increased sharply as the angle of inclination was increased. For $\theta < 70°$, the growth of the boundary layer was limited to the upstream locations, with the thickness remaining almost constant downstream. On the other hand, for $\theta > 110°$, the boundary layer grew so rapidly that it eventually separated from the plate. Obviously, the boundary layer concept may not be physically meaningful especially in the downstream locations when the plate is facing upward, i.e., when $\theta > 90°$.

4. ANALYTICAL MODEL

Referring to the physical system depicted in Figure 1, we are seeking among other features, a relation between the thickness, δ, of the two-phase gas bubble-liquid boundary layer and the distance, x, along the plate. The starting point of the analysis is the conservation laws for momentum and mass, the former to be applied simultaneously to both gas and liquid while the latter is to be separately applied to both phases. For the two-phase free-convection boundary layer, momentum, gas-mass and liquid-mass conservation, respectively, take the form

$$\alpha\rho_g \left(u_g \frac{\partial u_g}{\partial x} + v_g \frac{\partial u_g}{\partial y}\right) + (1-\alpha)\,\rho\left(u \frac{\partial u}{\partial x} + v \frac{\partial u}{\partial y}\right) = \frac{\partial \tau}{\partial y} + \alpha\,(\rho-\rho_g)\,g\cos(\theta-\pi/2) \qquad (1)$$

$$\frac{\partial}{\partial x}\left[\rho\,(1-\alpha)\,u\right] + \frac{\partial}{\partial y}\left[\rho\,(1-\alpha)\,v\right] = 0 \qquad (2)$$

$$\frac{\partial}{\partial x}\left[\rho_g\,\alpha\,u_g\right] + \frac{\partial}{\partial y}\left[\rho_g\,\alpha\,v_g\right] = 0\,. \qquad (3)$$

Nomenclature is given in Table 1. The buoyancy force, $\alpha\,(\rho - \rho_g)\,g\cos(\theta - \pi/2)$, in equation (1) is responsible for the motion of the two-phase boundary layer along the plate. It can be readily shown that the first term in equation (1), which represents the change in momentum of the gas bubbles, is quite small and need not be considered in the analysis.

We shall proceed to solve the above equations using an integral method. To do this, we have to postulate reasonable functional forms for the velocity and void fraction profiles. One possibility would be to apply the Prandtl-Nikuradse universal velocity profile for the liquid, assuming the existence of a turbulent core, a buffer zone, and an underlying laminar layer. This approach has met with some success in solving for the motion of the liquid phase in bubble columns [14], but in any case the exact forms of the profiles are not important in determining the physics of the model. The only essential assumption is that the profiles are similar at all x. Thus for the integration of equations (1) to (3), the following "top hat" velocity and void fraction profiles are assumed:

$$u(x,y) = \begin{cases} u(x) & 0 < y < \delta \\ 0 & y > \delta \end{cases} \qquad (4)$$

$$\alpha(x,y) = \begin{cases} \alpha(x) & 0 < y < \delta \\ 0 & y > \delta \end{cases} \qquad (5)$$

The above profiles have yielded good results for free convection plumes driven by air bubbling [8-10]. Note that in writing equations (4) and (5), both the liquid motion and the gas bubbles have been assumed to be confined to the same boundary layer with thickness $\delta(x)$. Equations (1) to (3) may now be integrated with respect to y to yield

$$\frac{d}{dx}\left[\rho(1-\alpha)\, u^2\, \delta\right] = -\tau_w + \rho\, \alpha\, \delta\, g \cos(\theta-\pi/2) \qquad (6)$$

$$\frac{d}{dx}\left[\rho(1-\alpha)\, u\, \delta\right] = \rho\, j_e \qquad (7)$$

$$\frac{d}{dx}\left[\rho_g \alpha u_g\, \delta\right] = \rho_g\, j_g \qquad (8)$$

where $\tau_w = \tau_w(x)$ is the wall shear stress at the plate, $\rho\, j_e$ the liquid mass flux swept into the boundary layer by turbulent entrainment, and $\rho_g\, j_g$ the mass flux due to gas injection through the plate. Since $\rho_g/\rho \ll 1$, we have assumed $(\rho - \rho_g) \sim \rho$ during the integration.

To close the above system, an independent expression is needed for the relative velocity. This is obtained by assuming that once the gas bubble releases from the porous surface, it instantaneously attains its terminal rise velocity. At any location then the gas velocity u_g depends only on the local void fraction α. The gas velocity relative to the liquid velocity is well described by an nth-order empirical equation of the form [13]

$$u_g - u = \left[V_\infty \cos(\theta-\pi/2)\right](1-\alpha)^{n-1} \qquad (9)$$

where V_∞ is the terminal velocity of a single bubble in undisturbed liquid and the index n is a phenomenological quantity which is a function of the regime of the bubbly flow. The quantity $[V_\infty \cos(\theta - \pi/2)]$ may be regarded as the characteristic velocity scale in the direction parallel to the plate. In the churn-turbulent regime, we have

$$n = 0 \text{ and } V_\infty = 1.53\left[\frac{\sigma g (\rho - \rho_g)}{\rho^2}\right]^{1/4} \qquad (10)$$

which yields a $V_\infty = 0.25$ m/s for an air bubble in water.

It is known from experiments with single phase turbulent boundary layers and jets that the entrainment velocity, j_e, is generally proportional to the mean flow velocity, where the proportionality constant E_o is the so-called entrainment coefficient. Some measurements of entrainment with gas jets having a density different than the ambient gas have been made by Ricou and Spalding [15]. They found that the entrainment rate varied with the square root of the ratio of the density of the jet to that of the surrounding gas. Accordingly, we have

$$j_e = \left[E_o \cos(\theta-\pi/2)\right]\left[\frac{(1-\alpha)\,\rho + \alpha\rho_g}{\rho}\right]^{1/2} \frac{\left[\alpha u_g + (1-\alpha) u\right]}{\left[\alpha u_g + (1-\alpha) u\right]} \qquad (11)$$

where $\cos(\theta - \pi/2)$ is employed to account for the effect of inclination. Since $\rho_g/\rho \ll 1$, equation (11) may be simplified as

$$j_e = \left[E_o \cos(\theta-\pi/2)\right](1-\alpha)^{1/2} \frac{\left[\alpha u_g + (1-\alpha) u\right]}{\left[\alpha u_g + (1-\alpha) u\right]} \qquad (12)$$

The above expression is essentially the two-phase one-dimensional version of the expression proposed by Morton [16] for turbulent jets driven by buoyancy. A similar expression has also been employed by Hussain and Seigel [8] for liquid jets pumped by rising gas bubbles. In earlier work on turbulent jets, Morton [17] found that if a top-hat velocity profile is used, $E_o = 0.116$ results in the best agreement between theory and experiment. This value of E_o will be employed in the numerical computation.

Finally, the equation for the shear stress at the wall will be taken directly from that for bubbly flow through vertical channels [13], namely

$$\tau_w = \frac{1}{2} C_f \frac{\left[\rho_g \alpha u_g + \rho (1-\alpha) u\right]}{\left[\alpha u_g + (1-\alpha) u\right]} \qquad (13)$$

where the friction factor is assumed to be a constant taken to be $C_f = 0.005$. The term $\rho_g \alpha u_g$ in the above expression is usually quite small compared with $\rho (1-\alpha) u$ and may be neglected.

END COLUMN HERE

END COLUMN HERE

FINAL COPY WILL BE REDUCED TO 77%

For convenience, the following dimensionless quantities are introduced:

$$\Delta = \delta\, g/V_\infty^2 \cos(\theta - \pi/2) \qquad (14)$$

$$X = xg/V_\infty^2 \cos(\theta-\pi/2) \qquad (15)$$

$$U = u/V_\infty \cos(\theta-\pi/2) \qquad (16)$$

$$J = j_g/V_\infty \cos(\theta-\pi/2) \qquad (17)$$

Substituting equations (9), (12), and (13) into equations (6) to (8), we obtain, in dimensionless form,

$$\frac{d}{dx}\left[(1-\alpha)\, U^2 \Delta\right] = -\frac{1}{2} C_f (1-\alpha) \qquad (18)$$

$$U\left[U + \alpha (1-\alpha)^{n-1}\right] + \alpha\Delta$$

$$\frac{d}{dx}\left[(1-\alpha)\, U\Delta\right] = \left[E_o \cos(\theta - \pi/2)\right] (1-\alpha)^{1/2} \left[U + \alpha(1-\alpha)^{n-1}\right] \qquad (19)$$

$$\frac{d}{dx}\left\{\alpha\left[U + (1-\alpha)^{n-1}\right]\Delta\right\} = J \qquad (20)$$

with initial conditions

$$\Delta(0) = \alpha(0) = U(0) = 0 \,. \qquad (21)$$

It can be shown that the following expressions which satisfy the initial conditions given by equation (21) are valid for $X \to 0$:

$$\Delta = aX^{2/3}, \quad \alpha = bX^{1/3}, \text{ and } U = cX^{2/3} \qquad (22)$$

where

$$c = \left(\frac{b}{2}\right)^{1/2} = \frac{2a}{3E_o} = \left(\frac{J}{3E_o}\right)^{1/3} . \qquad (23)$$

These small-X solutions are employed in the numerical solution of equations (18) to (20) using the Runge-Kutta method.

5. ANALYTICAL RESULTS—COMPARISON WITH EXPERIMENT

Computations of the two-phase boundary layer have been made for various sets of θ and J. As previously mentioned, the boundary layer concept does not apply to the case in which the plate is facing upward, i.e., $\theta > 90°$. Therefore, we shall be concerned only with the two-phase boundary layers along vertical and down-facing surfaces. The predicted growth of an argon gas-water boundary layer is shown in Figure 6 for $J = 0.4$. Also shown in the figure are the experimental data for comparison. Within the range of X explored, the boundary layer thickness may be roughly represented by $\Delta \sim X^m$, where the index, $0 < m < 1$, is a function of θ. The values of Δ predicted by the model are in good agreement with the experimental results when $\theta = 90°$. When $\theta < 90°$, the model overpredicts the boundary layer thickness, especially at large values of X. The difference between the theoretical and the experimental results becomes more significant as θ decreases from 70° to 45°. Physically, this is quite expected since the empirical equations for liquid entrainment and wall shear stress employed in the present analysis have been based largely on previous theoretical and experimental results for bubbly flow with a vertical orientation.

The effect of gas injection rate on the growth of the two-phase boundary layer along a vertical surface (i.e., $\theta = 90°$) is presented in Figure 7. The values of $J = 0.1$, 0.2, and 0.4 correspond to gas injection rates of 0.025, 0.05, and 0.10 m/s, respectively. As expected, a thicker boundary layer is obtained at a higher gas injection rate. Within the present experimental conditions, the local boundary layer thickness is found to increase according to the square root of the gas injection rate. Overall, the predicted values of Δ are in good agreement with the data. While the results shown in Fig. 7 are very encouraging, there is a real need for more experimental data to ensure that the previously developed assumptions and equations prove adequate. Future experiments should concentrate on gas bubbling or nucleate boiling on long vertical surfaces under conditions of free convection since there is virtually no information on this subject.

The predicted axial liquid velocity and void fraction versus axial distance along the plate are shown in Figure 8 for $\theta = 90°$ and $J = 0.2$. These quantities may be regarded as the values averaged over the thickness of the two-phase boundary layer since the results have been based on "top-hat" velocity and void-fraction profiles. We note from the figure that the void fraction exhibits a peak value near the leading edge of the boundary layer and then slowly decreases with distance along the plate. Although the value of α appears to be nearly the same at large values of X, the "local" void fraction may actually vary in the direction normal to the plate. The axial liquid velocity, on the other hand, increases rather rapidly in the upstream locations and then gradually decelerates downstream. It is interesting to note that the axial liquid velocity can become quite large compared with the relative velocity between gas bubble and liquid, or equivalently, compared with the terminal velocity, V_∞. The present results, however, need to be confirmed experimentally. While the use of the "top-hat" velocity profile seems to be adequate in modeling air-bubble plumes [8-10, 12], it may underestimate the wall effect in modeling two-phase boundary layers along solid surfaces.

END COLUMN HERE

FINAL COPY WILL BE REDUCED TO 77%

CONCLUSIONS

1. The behavior of the two-phase gas bubble-liquid boundary layer depends strongly on the gas injection rate and the angle of inclination.

2. Marked differences in the two-phase flow regime have been observed between up-facing and down-facing surfaces. These two cases must be modeled separately.

3. Rigorously, the boundary layer concept is valid only when θ is equal to or slightly less than 90°. Under this condition, the present model correctly predicts the two-phase boundary layer thickness.

4. For $0.1 < J < 0.4$ and $45° < \theta < 90°$, the boundary layer thickness may be roughly represented by $\Delta \sim J^{1/2} X^m$, where the index, $0 < m < 1$, is a function of θ.

5. More experimental data including velocity and void fraction measurements are needed to provide basic information for the development of a more elaborate model.

ACKNOWLEDGEMENTS

The authors wish to thank Marsha Mehaffey for typing the manuscript. The work was performed under the auspices of the U. S. Department of Energy while the first author was at Argonne National Laboratory.

REFERENCES

1. L. Baker, Jr., F. B. Cheung et al., Interaction of LMFBR core debris with concrete, Proceedings Post Accident Heat Removal Information Exchange Meeting, ANL-78-10 (1977) 223-232.

2. F. B. Cheung, D. R. Pedersen, and D. H. Nguyen, Modeling of core debris-sodium-concrete interactions, Proceedings Sixth Information Exchange Meeting on Debris Coolability, UCLA, 5 (1984) 21.1-21.10.

3. Y. Y. Hsu and J. W. Westwater, Approximate theory for film boiling on vertical surfaces, Chem. Engng. Prog. Symp. Ser., 56 (1960) 15-24.

4. E. M. Sparrow and R. D. Cess, The effect of subcooled film on laminar film boiling, J. Heat Transfer, 84 (1962) 149-156.

5. K. Nishikawa and T. Ito, Two-phase boundary-layer treatment of free-convection film boiling, Int. J. Heat Mass Transfer, 9 (1966) 103-114.

6. E. M. Greitzer and F. H. Abernathy, Film boiling on vertical surfaces, Int. J. Heat Mass Transfer, 15 (1972) 475-491.

7. L. Cumo et al., Two-phase boundary layer along heated walls, AIChE Symp. Ser., 73 (1977) 2-15.

8. N. A. Hussain and R. Siegel, Liquid jet pumped by rising gas bubbles, J. Fluids Engng., 98 (1976) 49-56.

9. N. A. Hussain and B. S. Narang, Analysis of two-dimensional air-bubble plumes, AIChE Journal, 23 (1977) 596-604.

10. T. J. McDougall, Bubble plumes in stratified environments, J. Fluid Mech., 85 (1978) 655-672.

11. J. H. Milgram, Mean flow in round bubble plumes, J. Fluid Mech., 133 (1983) 345-376.

12. N. A. Hussain and B. S. Narang, Simplified analysis of air-bubble plumes in moderately stratified environments, J. Heat Transfer, 106 (1984) 543-550.

13. G. B. Wallis, One-Dimensional Two-Phase Flow (McGraw-Hill, New York, 1969) 243-281.

14. K. Ueyama and T. Miyauchi, Properties of recirculating turbulent two-phase flow in gas bubble column, AIChE Journal, 25 (1979) 258-266.

15. F. P. Ricou and D. B. Spalding, Measurements of entrainment of axisymmetrical turbulent jets, J. Fluid Mech., 11 (1961) 21-32.

16. B. R. Morton, Modeling fire plumes, Tenth Symp. on Combustion, The Combustion Institute (1965) 973-986.

17. B. R. Morton, Forced plumes, J. Fluid Mech., 5 (1959) 151-163.

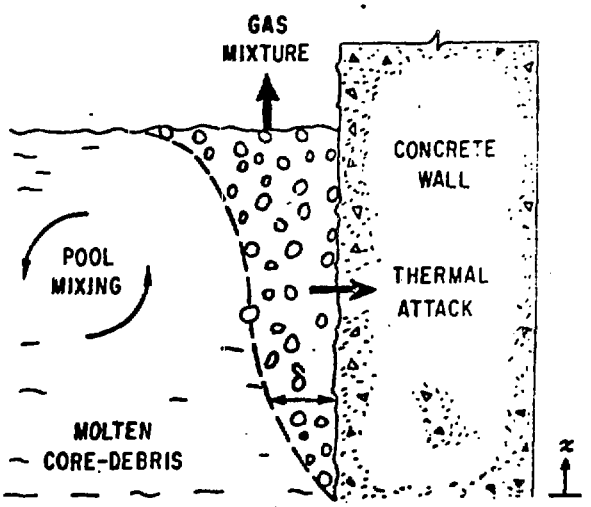

Fig. 1. Schematic of the physical system, showing the two-phase gas bubble-liquid boundary layer.

TABLE 1. Nomenclature

$a;b,c$	coefficients in equation (22)
C_f	friction factor, equation (13)
E_e	entrainment constant, equation (11)
g	acceleration due to gravity
j_e	liquid entrainment velocity
j_g	gas injection rate
J	dimensionless gas injection rate, equation (17)
n	an index employed in equation (9)
u	liquid velocity along the plate
u_g	gas velocity along the plate
U	dimensionless liquid velocity along the plate, equation (16)
v	liquid velocity normal to the plate
v_g	gas velocity normal to the plate
V_∞	terminal velocity, equation (10)
x	coordinate parallel to the plate
X	dimensionless axial coordinate, equation (15)
y	coordinate normal to the plate
δ	two-phase boundary layer thickness
Δ	dimensionless boundary layer thickness, equation (14)
θ	angle of inclination of the plate
τ	shear stress
τ_w	wall shear stress
σ	surface tension
ρ	liquid density
ρ_g	gas density
α	void fraction

Fig. 2. The gas injection unit and the two-phase free-convection boundary layer along an up-facing surface (θ = 110°).

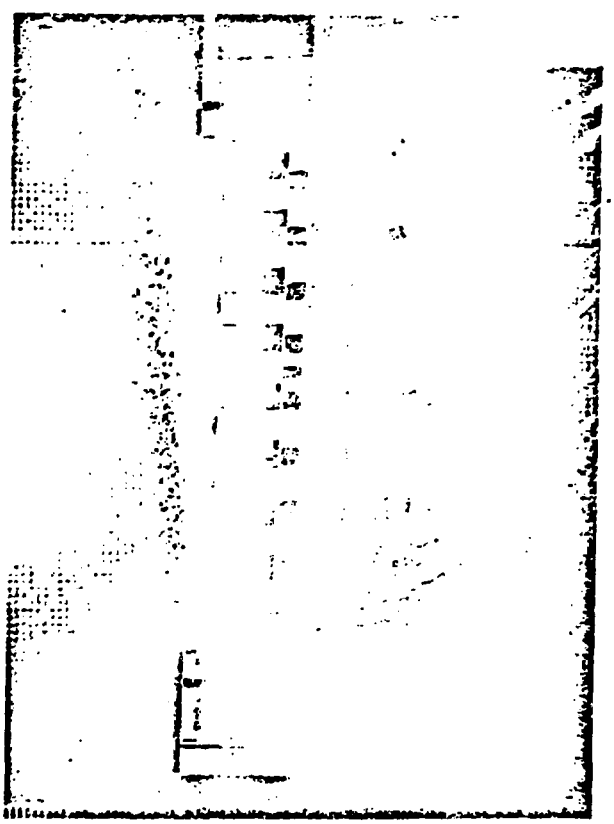

Fig. 3. Development of the two-phase free-convection boundary layer along a vertical surface (θ = 90°).

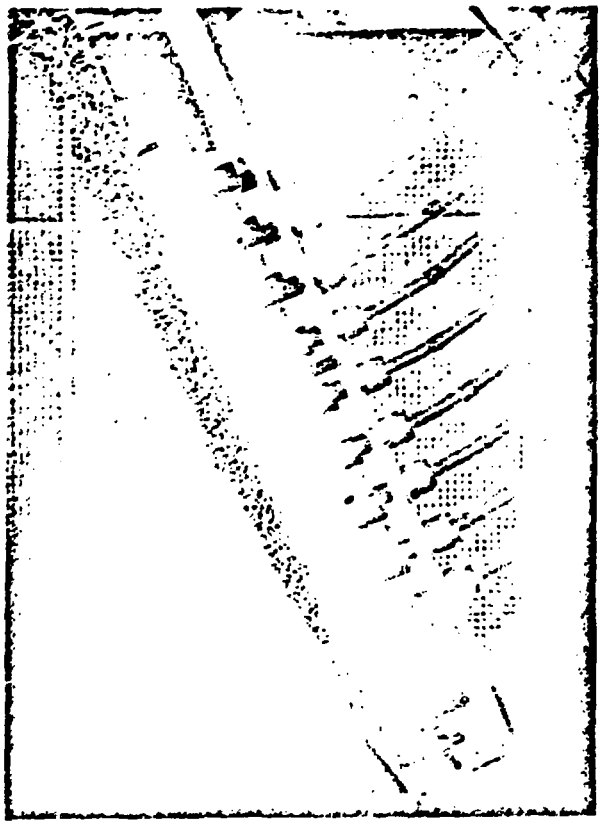

Fig. 4. Development of the two-phase free-convection boundary layer along a down-facing surface (θ = 70°).

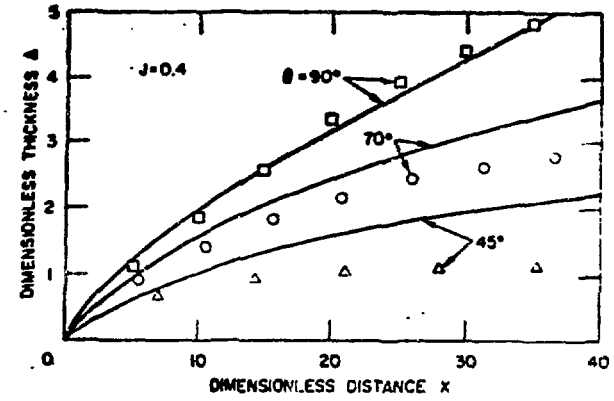

Fig. 6. The predicted and the measured thicknesses of the argon gas-water boundary layer at various angles of inclination (J = 0.4).

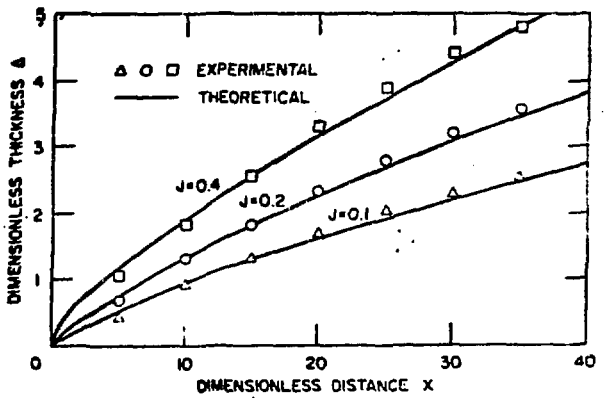

Fig. 7. The predicted and the measured thicknesses of the argon gas-water boundary layer at different gas injection rates (θ = 90°).

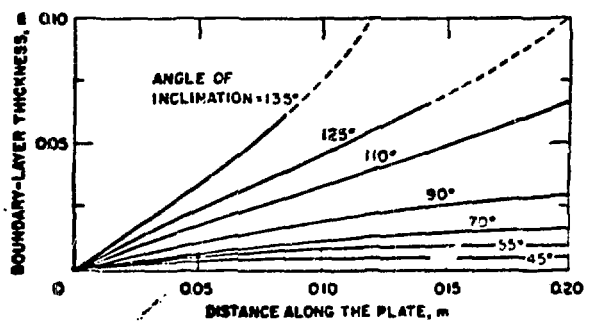

Fig. 5. The experimentally observed boundary layer thickness along the plate at different angles of inclination (j_g = 0.10 m/s).

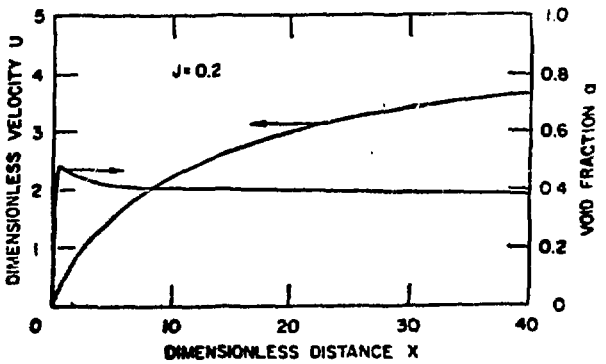

Fig. 8. Axial variations of the liquid velocity and void fraction along a vertical surface.